Since the parameter b in (15) approaches 1 as the electron energy approaches its maximum $W_0 - m_\nu^2/2m_\mu$, the relative sensitivity of μ decay to a and m_ν is different from that of processes (3) and (4). To take the example of the last paragraph but one, if $a=0$ and $m_\nu=1.6$ MeV, the parameter b would affect both the energy spectrum and the asymmetry, for electron energies near the maximum, by an amount that might be observed by an improvement of existing measurements. But if $a=0.02$ and $m_\nu=0$, the parameter a^2 in (15) would be quite negligible. Thus, an improved measurement of the tail of the electron spectrum in μ decay might be combined with a measurement of the branching ratios for (3) and (4) to give an estimate of both a and m_ν.

The preceding considerations are theoretical. In the immediate future, however, there is little hope of observing reactions (3) and (4) unless the branching ratio R_3/R_1 is at the least 0.01. Such a large effect could not be produced by m_ν alone and could only be interpreted as evidence that $a^2>0$. Indeed, it is known from the energy-momentum balance in π-μ decay[6] that

$m_\nu \lesssim 3\frac{1}{2}$ MeV. From Eq. (13) it follows that if $a=0$, R_3/R_1 is at most about 1/200.

An upper limit on a^2 may be obtained from the isotropic energy spectrum of the electrons in μ decay. If we neglect m_ν, the ρ value from Eq. (15) is $\frac{3}{4}(1+a^2)^{-1}$. Plano's[7] experimental value is 0.780 ± 0.025. If this is taken literally it is too high even if $a^2=0$. Let us therefore allow two standard deviations; then $\rho \geqslant 0.730$, $a^2 \leqslant 0.027$, and $R_3/R_1 \lesssim 5\frac{1}{2}/100$.

The maximum conceivable value of R_3/R_1 is obtained by letting a be positive and giving m_ν and a^2 their maximum values. Let us neglect the influence of $m_\nu \approx 3\frac{1}{2}$ MeV on the ρ value in μ decay, so that we can retain our maximum of 0.027 for a^2. Then the maximum value for R_3/R_1 is about 8/100.

[6] W. H. Barkas, W. Birnbaum, and F. M. Smith, Phys. Rev. 101, 778 (1956).

[7] R. Plano, Phys. Rev. 119, 1400 (1960).

π⁻-p Elastic Scattering at 310 MeV: Differential Cross Section and Recoil-Proton Polarization*

Hugo R. Rugge† and Olav T. Vik‡

Lawrence Radiation Laboratory, University of California, Berkeley, California

(Received 4 October 1962)

The differential cross section and recoil-proton polarization in π^--p elastic scattering at 310-MeV incident-pion energy has been measured. The differential cross section was measured at 28 angles in the angular region $25 \leqslant \theta_{lab} \leqslant 160$ deg. The fractional rms errors were typically 3%. The reaction was observed by counting the scattered pions emerging from a liquid-hydrogen target with a counter telescope consisting of scintillation and Čerenkov counters. Simultaneously, the recoil-proton polarization was measured at four angles in the angular region $114 < \theta_{c.m.} < 146$ deg. The recoil protons from the liquid-hydrogen target were scattered from a carbon target and the left-right asymmetry was measured. Scintillation counters were used throughout to detect the particles.

I. INTRODUCTION

THE pion-nucleon interaction has been experimentally studied for some time. In the majority of the experiments performed, differential and total cross sections for the elastic scattering of positive and negative pions on protons have been measured. Although there exists a reasonable amount of data, most of it lacks completeness and accuracy at any single energy, especially in the region near 300 MeV. The experiments described herein are a part of a continuing effort at the Lawrence Radiation Laboratory to obtain accurate and complete data on the π-N interaction at 310 MeV. Previously Rogers et al.[1] had made accurate measurements of the differential cross section for π^+-p elastic scattering, and Foote et al.[2] had obtained recoil-proton polarization for the same reaction. However, investigation of π^+-p scattering leads only to information about the isospin 3/2 state of the π-N system. To

[1] E. H. Rogers, O. Chamberlain, J. Foote, H. Steiner, C. Wiegand, and T. Ypsilantis, Rev. Mod. Phys. 33, 356 (1961).
[2] J. Foote, O. Chamberlain, E. Rogers, H. Steiner, C. Wiegand, and T. Ypsilantis, Phys. Rev. 122, 948 (1961).

obtain information about the isospin 1/2 state, the $\pi^- - p$ interaction must be studied. For this reason we have made measurements of the elastic scattering of negative pions on protons:

$$\pi^- + p \rightarrow \pi^- + p.$$

The analysis of π-N scattering data is usually made in terms of phase shifts. In past analyses, ambiguities in phase-shift solutions have arisen. Measurements of the polarization of the recoil proton have been shown to be useful in removing these. We have, therefore, measured the recoil-proton polarization at several angles, and have also made an accurate measurement of the differential cross section.

To significantly improve existing data, it was necessary to develop a pion beam of high intensity; for this purpose a 3×10^6 π^-/sec beam was obtained at the 184-in. synchrocyclotron. A description of the pion beam, and the methods and results of both the differential cross section and polarization measurements, follows.

II. PION BEAM

The ultimate success of these experiments depended upon having a very intense 310-MeV π^- beam available. Because of the importance of this beam to the experiments, we devote this section to a detailed account of its design and final characteristics.

A. Design

After a short preliminary run had shown that π^- beams produced by the external proton beam of the 184-in. synchrocyclotron were unsatisfactory, especially for polarization measurements, a study was made of possible internally produced pion beams in the 300-MeV energy region. A mechanical orbit plotter was used to trace the trajectory of the pion in the cyclotron field.

Negative π mesons were produced by inserting a beryllium target into the 740-MeV internal proton beam of the 184-in. synchrocyclotron (see Fig. 1). The pions produced at 0 deg were deflected out of the cyclotron by its own magnetic field, and passed through a thin aluminum window in the vacuum tank and into the 8-in. aperture of the two-section (doublet) quadrupole magnet, Q_1. This quadrupole formed a parallel beam that passed into an 8-ft-long iron collimator known as the meson wheel. From the wheel the beam entered the experimental area known as the meson cave, where it then entered another focusing quadrupole magnet Q_2. This magnet also had an 8-in. aperture and two sections. Upon leaving Q_2 the beam was momentum analyzed by a bending magnet M_1. The angle of deflection chosen was 36 deg, to compensate for the momentum dispersion in the pion beam introduced by the cyclotron field. The combined effect of Q_2 and M_1 was to focus an image of the pion source on the liquid-hydrogen target.

An IBM 650 program DIPOLE was developed, which applied simple lens formulas to the two sections of the

TABLE I. Counters used in the differential cross-section measurement.

Counter No.	Type	Light guide or pipe	Size	Thickness (in.)
B_1	Plastic scint.	Alum.	4-in. diam	1/8
B_2	Plastic scint.	Alum.	3-in. diam	1/16
S_1	Plastic scint.	Alum.	4-in. diam	1/16
S_2	Plastic scint.	Lucite	$2\frac{1}{4}$-in. diam	1/4
S_3	Plastic scint.	Lucite	12×12 in.	3/4
C_1	H_2O Čerenkov	Lucite	4×4 in.	$1\frac{1}{2}$

doublet quadrupoles, and thus calculated current settings. The current in the bending magnet M_1 was accurately determined by the suspended-wire technique, which was also used to check the currents in Q_2. Fine tuning of the focusing magnets was done with the pion beam and the beam profile counters described below.

III. DIFFERENTIAL CROSS-SECTION MEASUREMENT

The 310-MeV π^- beam described above impinged on a 6-in.-diam liquid-hydrogen target. For most of the measurement the beam was monitored with an argon-filled ionization chamber. The pions scattered by the hydrogen were detected with a counter telescope consisting of two plastic scintillation counters and a Čerenkov counter. During part of the measurement, the incident-pion beam was monitored by a pair of scintillators in order to obtain a more accurate normalization of the differential cross section, which was measured at a total of 28 angles.

A. Experimental Arrangement and Apparatus

Most of the counters used in the differential cross-section measurement were composed of polystyrene plastic scintillator and were viewed with RCA 6810A photomultiplier tubes. The exception was the liquid Čerenkov counter, C_1. Lucite light pipes or aluminum (Alzak) light guides were used to guide the light to the phototube on all the counters. The Čerenkov counter
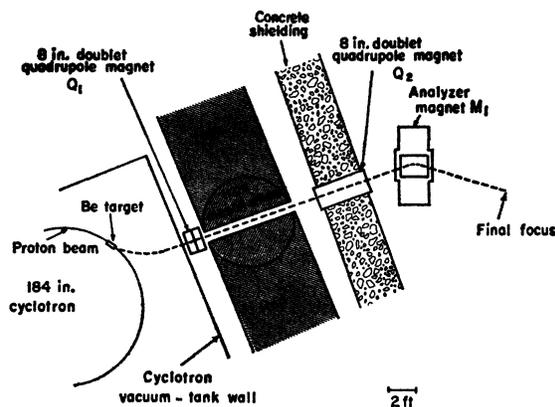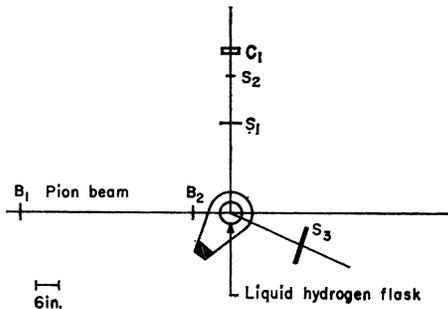

FIG. 1. Beam layout.

FIG. 2. Scale drawing (plan view) of counter and target arrangement used to measure differential cross section.

was a rectangular box with $\frac{1}{8}$-in. Lucite walls, filled with water. Data concerning the counters are found in Table I. The positions of the counters used in the differential cross-section measurement are shown in Fig. 2. Not all of the counters shown were used in every phase of the measurement.

B. Beam Characteristics

The elements of the magnet system were placed in their calculated positions, and the flux through a 7-in.-diam argon-filled ionization chamber, placed at the final focus, was then optimized by varying the radial and azimuthal settings of the internal target as well as the target material. The target finally used was beryllium, 2 in. high, $\frac{1}{2}$ in. radially, and lying 1 in. along the beam direction. Helium bags placed throughout the accessible length of the magnet system reduced multiple scattering. The final beam had the characteristics:

Intensity (maximum)	3×10^6 π^-/sec
Mean energy	310 MeV
Energy half-width	5 MeV
Image full width at half-max:	
Horizontal	4.2 cm
Vertical	3.2 cm
μ^- contamination	4.5%
e^- contamination	<0.3%

The μ^- contamination was determined from an integral range curve of the beam. A gas Čerenkov counter filled with sulfur hexafluoride was used to measure the e^- contamination.[3]

The position of the final focus was extremely sensitive to the radial setting of the internal target. Calibration of the radial target position was insufficiently accurate to allow the cyclotron operator to set the target properly at the start of each day's operation. For this reason we had to determine the radial target position experimentally at the start of each run. This was accomplished by sweeping a pair of $\frac{1}{4}$-in.$\times\frac{1}{4}$-in. scintillation counters across the beam and thus measuring the beam profile. A constant check on possible beam shifts during runs

[3] J. H. Atkinson and V. Perez-Mendez, Rev. Sci. Instr. 30, 865 (1959).

was made by observing the ratio of counting rates in M_1 and M_2. This is discussed in Sec. IVA.

After leaving the magnet system, and before striking the hydrogen target, the pion beam passed through a 10-in.-long brass collimator surrounded by lead. This collimator was designed to attenuate the spatial components of the pion beam which were directed toward the heavy aluminum flanges supporting the liquid-hydrogen target. These components were the main source of coincidence counts in the differential cross-section measurement with the hydrogen flask empty. The collimator was used only when the incident beam was monitored by the ionization chamber.

The two scintillation counters S_1 and S_2, and the Čerenkov counter C_1, were grouped together into a rigid counter telescope system with relative positions as shown in Fig. 2. The liquid selected for the Čerenkov counter, C_1, was water, which gives Čerenkov light when traversed by charged particles having $\beta \geqslant 0.75$.

A threshold of $\beta = 0.75$ allows the telescope to reject all protons and most inelastic pions. It does not, however, reject the most energetic charged inelastic pions at forward angles. For this reason, at angles forward of 70 deg in the lab system, copper absorber was placed before counter C_1 to degrade the energy of the most energetic inelastic pions, so that their velocity was below the threshold of the counter. The introduction of copper absorber into the counter telescope at forward angles, because of nuclear attenuation and Coulomb scattering, reduced the number of elastically scattered pions in the telescope.

To be able to correct for this reduction, measurements of telescope efficiency in the angular region of interest were carried out. The counter telescope was placed in the incident-pion beam at low intensity. This incident beam was then degraded in energy, using copper absorber, to a number of different energies corresponding to the energies of elastically scattered pions at lab angles from 25 through 70 deg. At each setting the appropriate amount of copper was placed in front of counter C_1 in the counter telescope, and measurement of the ratio $S_1S_2C_1/S_1S_2$, was made at that incident energy. The efficiency was determined from the ratio following suitable corrections for contaminants in the incident and scattered beams.

At three of these energies, integral range curves were taken of the incident beam, both to check its energy and to determine the muon contamination. Values of muon contaminations at other energies were interpolated from a curve of the three points obtained from these range curves.

A list of the amount of copper used at each angle, and the calculated efficiency at that angle, is given in Table II. Measurements of the scattering out of pions by counter S_2, and the efficiency of the Čerenkov counter, were also obtained by recording the $S_1S_2C_1/S_1S_2$ ratio with no copper in the counter telescope.

TABLE II. Forward-angle-counter telescope efficiencies.

θ_{lab} (deg)	Efficiency	Amount Cu in telescope (g/cm^2)
25	0.802	33.6
30	0.850	25.5
35	0.867	22.6
40	0.890	16.7
45	0.918	13.9
50	0.955	8.6
55	0.967	5.4
60	0.976	3.7
65	0.978	3.3
70	1.00	0.0

Our electronics arrangement employed a coincidence circuit of the Garwin type[4] to detect scattered events of interest. The output pulses from the photomultipliers were delayed and amplified when necessary. The properly delayed pulses from all the counters were fed into the multi-input coincidence curcuit. The output pulses of the coincidence circuit were fed into 10 Mc/sec discriminating units that, in turn, drove conventional scaling units. The resolving time of the system was approximately 20×10^{-9} sec. The appropriate counter voltages and delays were determined experimentally by optimizing the coincidence rate with respect to these variables. This was done in the incident-pion beam at low intensity. These settings were checked at a number of different scattering angles during the experiment. The current from the ion chamber which monitored the incident-pion beam was transmitted to a standard integrating electrometer by double-shielded cable, and displayed on a recorder. A scaler-gater unit was used to turn the ion chamber electrometer and all scaling units on or off simultaneously.

The liquid-hydrogen target consisted of an upright cylinder 6 in. in diameter and 8 in. high, made of 0.010-in. Mylar and encased in a vacuum jacket 12 in. in diameter. At beam level, the vacuum jacket consisted of 0.030-in. Mylar windows 6 in. high, supported above and below beam level by $\frac{1}{2}$-in. Dural flanges. The Mylar extended around for 270 deg, making it possible to measure the recoil-proton polarization simultaneously with the differential cross-section measurement. In order to measure the target-empty rate, the liquid hydrogen was forced out of the target and back into the reservoir by introducing helium gas at the top of the hydrogen container. The level of hydrogen both in the target and in the hydrogen reservoir was monitored by magnehelic gauges that measured pressure differential between the top and the bottom of the target.

C. Experimental Procedure

1. Accidentals and Background

Accidentals in the counter telescope were measured in the usual manner. Each counter in the telescope was

delayed in turn, with respect to the remaining counters, by 54×10^{-9} sec (the time difference between two successive cyclotron rf pulses). The accidental coincidence rate of the telescope was found to be $<0.1\%$ of the true counting rate at all angles, and hence negligible.

The most important source of background comes from the scattering of pions in the walls of the hydrogen-containing flask and surrounding material. This background can be measured by emptying the flask of hydrogen and measuring the target-empty rate. This rate varied over different scattering angles from approximately 25 to 50% of the target-full rate.

A more difficult background to measure is that from contamination by electrons (the term electrons is used throughout this paper to mean both positrons and negative electrons unless otherwise noted) in the scattered pion beam. These electrons result because the production of neutral pions in the charge-exchange reaction [Eq. (1)] takes place in the liquid hydrogen. The subsequent decay of the π^0 produces the electrons

$$\pi^- + p \rightarrow \pi^0 + n; \tag{1}$$

$$\pi^0 \rightarrow \gamma + \gamma \tag{2}$$

or

$$\pi^0 \rightarrow \gamma + e^+ + e^-. \tag{3}$$

The electron background arises from the two decay modes of the π^0 indicated above because the counter telescope cannot distinguish between an electron and an elastically scattered pion. In the first [Eq. (2)], the two gammas may interact with the hydrogen and surrounding materials to produce electron-positron pairs. In the second decay mode [Eq. (3)], the $e^+ + e^-$ pair is produced directly in the π^0 decay (Dalitz pair).[5]

The magnitude of the electron background for both π^0 decay modes can be calculated with sufficient accuracy if the charge-exchange cross section is known at 310 MeV. We calculated this background using the charge-exchange data of Caris et al. at 317 MeV.[6] The background due to the usual decay of the π^0 [Eq. (2)], which for convenience we call "conversion electrons," can be calculated from the charge-exchange differential cross section,[6] the pair production cross sections for the various materials between the hydrogen target and the counter telescope,[7] and the opening-angle distribution of the electron-positron pairs.[8] Background due to Dalitz pair production, for convenience called "Dalitz electrons," can similarly be calculated with the charge-exchange cross section,[6] the branching ratio of the π^0 decay,[9] and the opening angle distribution of the Dalitz electron pairs.[9,10]

[4] R. L. Garwin, Rev. Sci. Instr. 21, 569 (1950).

[5] R. H. Dalitz, Proc. Phys. Soc. (London) A64, 667 (1951).
[6] J. C. Caris, R. W. Kenney, V. Perez-Mendez, and W. A. Perkins, Phys. Rev. 121, 893 (1961).
[7] J. H. Atkinson, Jr., and B. H. Willis, Lawrence Radiation Laboratory Report UCRL-2426, 1957 (unpublished), Vol. II, p. 65.
[8] A. Borsellino, Phys. Rev. 89, 1023 (1953).
[9] D. Josephs, Nuovo Cimento 16, 997 (1960).
[10] M. Derrick, J. Fetkovich, T. Fields, and J. Deahl, Phys. Rev. 120, 1022 (1960).
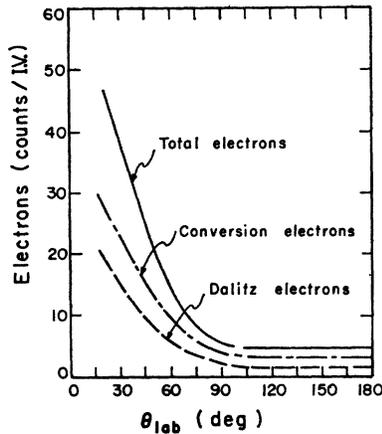
FIG. 3. Electron contamination in the scattered pion beam as a function of laboratory-system scattering angle.

The results of these calculations are shown in Fig. 3. Figure 4 is a "smooth" fit to the measured differential cross section in the same units, for comparison.

It was possible to make some experimental checks on the calculated electron contamination described above. The first source of background is due to the conversion of γ rays in the target and surrounding material, and is therefore proportional to the amount of material between the scattering point and the counter telescope. Approximately 1% of the γ's coming from the target are converted into pairs by this material.

The calculation on conversion electrons was checked by increasing the amount of converting material between the target and counter telescope. From one to five 0.15-g/cm² sheets of copper were placed next to the target, and the counting rates in the counter telescope obtained for each case with the liquid-hydrogen target both full and empty. Each copper sheet converted roughly the same number of γ's from the charge-exchange reaction as did the target without copper. By extrapolating a curve of the counting rate vs "effective target thickness" to zero target thickness at several angles, the conversion-electron contamination could be determined with fair accuracy at these angles. The measured values agreed well with the calculated values.

The second source of background is the Dalitz pairs. No direct measurement of this contamination was made, but a check on the total background from charge-exchange scattering was obtained by putting a conjugate counter in coincidence with the counter telescope. This counter (S_3) was placed at an appropriate angle on the other side of the target to detect the proton conjugate to the elastically scattered pions counted in the counter telescope. Essentially none of the electrons can duplicate this coincidence between the conjugate counter and counter telescope; hence, a comparison of rates with and without the conjugate counter in coincidence can give the contamination at those angles where the measurement can be made. The size of S_3, fixed by the geometry of the target and counter telescope, prohibits measurements from being at pion lab angles

much greater than 100 deg, because S_3 then partially intercepts the incident pion beam and is jammed by it. At forward pion angles (S_3 angles near 90 deg lab), the protons either do not get out of the target or are badly multiply scattered. For these reasons, measurements could only be made near 90-deg pion lab angles. Those made were in agreement with the calculation of the total electron contamination.

2. Cross-Section and Normalization Measurement

Data for the cross-section measurement were taken at 28 lab scattering angles from 25 to 160 deg in 5-deg steps. The incident beam was monitored by a 7-in.-diam argon-filled ionization chamber, and the scattered pions were detected by the counter telescope $S_1S_2C_1$. The data were taken in cycles of hydrogen target full and empty. Ordinarily, several such cycles were completed and then the counter telescope was moved to a different angle. At several angles, voltage plateaus of all counters were checked. The accidentals mentioned previously were checked with target full and empty and found to be negligible at all angles. Data were taken at several angles with the counter telescope at varying distances from the target, thus giving a solid angle other than the "normal" one. The value of the cross section obtained in this way was in agreement with the value with data taken at the "normal" solid angle. Data taken at full beam level were checked at lower beam levels throughout the duration of the experiment and found to be independent of beam level.

A pion beam of intensity greater than 10⁶ pions/sec was necessary to achieve the accuracy desired in the differential cross-section measurement. Such an intense beam cannot be counted by scintillation counters be-
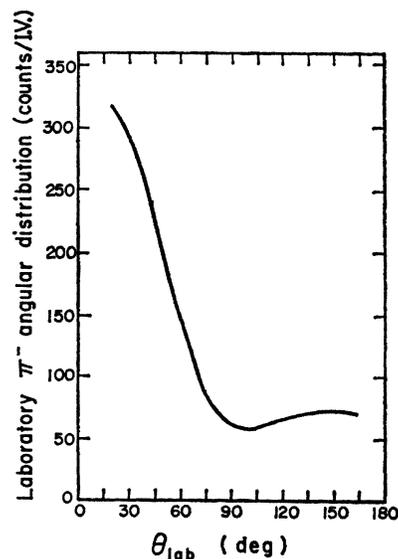

FIG. 4. Smooth curve of lab-system π^- angular distribution vs scattering angle.

TABLE III. Normalization run, differential cross-section data.

θ_{lab} (deg)	$\theta_{\text{c.m.}}$ (deg)	Normalization $(d\sigma/d\omega)_{\text{c.m.}}$ (mb/sr)
50	66.8	0.948±0.029
90	109.8	0.447±0.019
145	155.2	0.941±0.022

cause counting losses are prohibitive with the usual cyclotron duty cycle and present μsec resolving times of coincidence circuitry. Therefore, as mentioned above, the differential cross-section data were taken while the incident pion beam was being monitored with an ionization chamber. It was felt, however, that if accurate measurements of the differential cross section could be made at a few angles while monitoring the incident beam with counters, this would allow more accurate determination of the over-all normalization of the differential cross section than with the ionization chamber alone.

Such a measurement became feasible with the completion of the auxiliary dee of the Berkeley 184-in. cyclotron, which increases the duty cycle by roughly a factor of 25, which in turn allows much higher counting rates in beam counters with negligible counting losses.

No changes were made in the beam or target during the normalization run. The ionization chamber was replaced by counters B_1 and B_2 as shown in Fig. 2. The dimensions of the counters are given in Table I. The signals from counters B_1 and B_2 were delayed with respect to the counter telescope and amplified. They were then fed into a Wenzel-type coincidence[11] with an 8×10^{-9} sec resolving time. The output of the coincidence circuit was amplified and then split, half the signal driving a 40-Mc/sec discriminator-scaler unit, and the other half being put into coincidence with the counter telescope in the Garwin-type coincidence circuit.[3] The output of this circuit was fed into a 10-Mc/sec discriminator unit that, in turn, fed uniform pulses to 10-Mc/sec scaler units.

During the experimental run the counting rate in beam counters was varied from about 1 to 3×10^5 π/sec. The beam time characteristics and the scaler gating were continuously displayed on a dual-beam oscilloscope. Periodic checks of counting losses were made by delaying counter B_1 with respect to counter B_2 by 54×10^{-9} sec. The counting losses were always $\leqslant0.1\%$ of the counting rate. Cross-section measurements were made with the counter telescope at three lab scattering angles of 50, 90, and 145 deg.

Each cycle consisted of a target-full and target-empty run, and a run on both a full and empty target with the beam counters delayed by 54×10^{-9} sec with respect to the counter telescope. This coincidence rate measured the accidental rate between the telescope and beam

[11] W. A. Wenzel, University of California Radiation Laboratory Report UCRL-8000, 1957 (unpublished).

counters. A correction to the data was made for this accidental rate, which was less than 2% of the normal counting rate at all angles.

A list of cross-section data obtained in this normalization run is given in Table III.

D. Results and Errors

Several corrections must be made to the raw data before a differential cross section can be extracted from it. One purpose of the measurement was to keep these corrections as small as possible, consistent with the performance of the polarization measurement discussed in Sec. IV of this paper. The largest corrections were for background. The target-empty rate was subtracted from the target-full rate at each angle, to obtain the counting rate due to hydrogen alone and the electron background was then subtracted from this hydrogen rate. A correction was also made for the telescope efficiency. In addition to the correction for copper in the telescope at angles forward of 70 deg lab, a further correction had to be applied for pions scattered out by the telescope counters themselves. This efficiency varied from 98.5 to 97% for all angles at which data were taken. Additional corrections, each less than 1% of the effect, were made for finite sizes of the target and defining counter for the counter telescope, rescattering in hydrogen of a once-scattered pion, multiple scattering, etc. All these corrections were also applied to the normalization run data. A further correction was made for the contamination of muons and electrons in the incident-pion beam.

The lab differential cross section is related to the average scattered pion per incident pion, N_s/N_i, by the equation

$$d\sigma(\theta)/d\Omega = N_s(\theta)/N_i\Omega T, \qquad (4)$$

where N_i is the number of incident pions, and N_s is the number of pions scattered into a counter that subtends a solid angle Ω as seen from the target, and lying at an angle θ with respect to the incident pion direction. The target constant T is the effective thickness of the target in protons/cm^2. During most of the experiment, Ω was equal to 2.70×10^{-3} sr. The target constant T was 6.16×10^{23} protons/cm^2.

In order to obtain a more accurate normalization of the cross-section data than that obtained with the ion chamber, the 28 angular distribution points measured while monitoring the incident beam with the ion chamber were transformed into the center-of-mass system, as were the 3 differential cross-section points obtained with scintillation counters monitoring the incident pion beam. A least-squares fit of a power series in $\cos\theta_{\text{c.m.}}$ (where $\theta_{\text{c.m.}}$=c.m. angle) was made to the 28 c.m. angular distribution points. This resulted in a smooth "best-fit" curve for all c.m. angles. The values of the angular distribution points in units of counts per integrated volt (one I.V.$=10^{-8}$ coulomb of charge
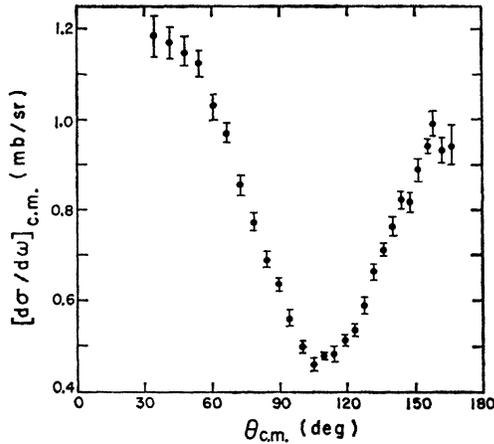
FIG. 5. 310-MeV π^- differential cross section plotted vs scattering angle in the center-of-mass system.

TABLE IV. π^--p differential cross section in the center-of-mass system.

θ_{lab} (deg)	$\theta_{c.m.}$ (deg)	Differential cross section (mb/sr)	Percentage error due to counting statistics only
25	34.7	1.184±0.043	2.5
30	41.4	1.171±0.035	1.4
35	47.9	1.151±0.033	1.5
40	54.4	1.125±0.029	1.5
45	60.6	1.027±0.027	1.7
50	66.8	0.970±0.023	1.4
55	72.7	0.853±0.023	1.8
60	78.5	0.774±0.018	1.6
65	84.1	0.690±0.018	2.1
70	89.6	0.635±0.015	1.9
75	94.9	0.561±0.017	2.6
80	100.0	0.498±0.013	2.2
85	105.0	0.461±0.014	2.7
90	109.8	0.480±0.009	1.5
95	114.5	0.482±0.016	2.9
100	119.0	0.514±0.012	1.8
105	123.5	0.536±0.013	2.0
110	127.8	0.590±0.018	2.7
115	132.0	0.663±0.019	2.5
120	136.0	0.715±0.016	1.9
125	140.0	0.764±0.021	2.7
130	144.0	0.822±0.020	2.3
135	147.8	0.817±0.021	2.4
140	151.6	0.889±0.025	2.7
145	155.2	0.941±0.015	1.4
150	158.9	0.991±0.028	2.5
155	162.4	0.932±0.029	2.7
160	166.0	0.944±0.042	4.2

collected from the ionization chamber) were taken from this curve at the three angles where the normalization differential cross-section measurement had been made. The average value of the ratio (counts/I.V.)/(mb/sr), obtained at each of the three angles, was used to normalize the angular distribution.

An absolute calculation of the differential cross section was also made by using the ionization chamber alone. The absolute scale of the differential cross section measured with the ionization chamber had an uncertainty of about 6%, while the normalization procedure described above resulted in about a 3% uncertainty in the absolute scale factor. The scale factor as determined by the ionization chamber differed from that determined by the normalization procedure by 3.5%.

A list of differential cross section vs c.m. scattering angle is given in Table IV. A graph of the data is shown in Fig. 5.

The uncertainties associated with the differential cross-section measurements fall into three natural categories: (a) counting statistics, (b) absolute differential cross-section scale, and (c) corrections. The counting statistics were determined in the usual manner, through the formula

$$\Delta(N_s/N_i) = \{[N_s(\theta)/N_i^2]_{full} + [N_s(\theta)/N_i^2]_{empty}\}^{1/2}. \quad (5)$$

A list of percentage error in the differential cross section due to counting statistics is found in the last column of Table IV. The error in the absolute cross-section scale resulted mainly from statistical counting errors on the normalization points and uncertainty in the target constant. The error in the determination of the solid angle is negligible.

A parameter ϵ was introduced to express the uncertainty in the absolute differential cross-section scale. The data are thus presented as $(d\sigma/d\omega)(1+\epsilon)$, where the most probable value of ϵ is zero. The error on ϵ is estimated to be 3%.

Errors due to various corrections to the data are the most difficult to estimate. The main uncertainty comes from the calculation of the electron contamination in the scattered pion beam. It was estimated that because of uncertainties in the data used and approximations made, an error of between 15 and 20% of the magnitude of the correction should be attached to this calculation. The uncertainties in the corrections for telescope efficiency, finite counter, and target size, etc., result in essentially negligible errors for most of the differential cross-section points; however, the corrections themselves have been included in determining the magnitude of the differential cross section. The errors quoted in the differential cross-section points in Table IV are an rms combination of the counting statistical error and the electron contamination error.

A measurement of the total cross section was also carried out but is not discussed in this report. A transmission measurement was made as a function
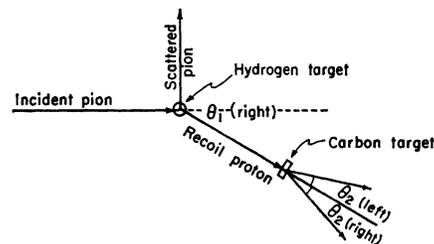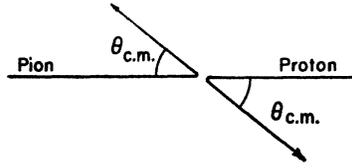

FIG. 6. Scattering geometry defined in conjunction with Eq. (8).

FIG. 7. Center-of-mass scattering geometry.

of cutoff angle.[12] The analysis of these data by a phase-shift program (see following paper by the authors, "Pion-Nucleon Scattering at 310 MeV: Phase-Shift Analysis") led to the value of 27.7 ± 0.7 mb, in good agreement with values obtained by other experimenters at this energy.[13]

IV. POLARIZATION MEASUREMENT

This section reviews briefly the standard method of measuring polarization, and describes the apparatus used. The experimental procedures are outlined and the results and uncertainties quoted.

A. Method and Apparatus

1. Method

In order to measure the polarization of a given beam of particles, one may utilize scattering from a spin-zero material, in our case carbon. The differential cross section for scattering a beam of particles of polarization P_1 directed along some unit vector $\hat{n}_1$ is given by[14]:

$$\frac{d\sigma}{d\Omega}(\theta) = \left[\frac{d\sigma}{d\Omega}(\theta)\right]_0 [1 + P_1 P_2(\theta)\hat{n}_1 \cdot \hat{n}_2], \quad (6)$$

where

$$\left[\frac{d\sigma}{d\Omega}(\theta)\right]_0$$

is the differential cross section for an unpolarized beam scattering through an angle θ, $P_2(\theta)$ is that polarization that would result from scattering an unpolarized beam through an angle θ, and the unit vector $\hat{n}_2$ is defined by:

$$\hat{n}_2 = \mathbf{k}_{\text{inc}} \times \mathbf{k}_{\text{scatt}} / |\mathbf{k}_{\text{inc}} \times \mathbf{k}_{\text{scatt}}|.$$

If the scattering is in the plane perpendicular to the unit vector $\hat{n}_1$, then the quantity $\hat{n}_1 \cdot \hat{n}_2$ is ± 1. We have the quantity

$$\text{Asymmetry} \equiv e(\theta) \equiv \frac{I_L(\theta) - I_R(\theta)}{I_L(\theta) + I_R(\theta)}, \quad (7)$$

where

$$I_L(\theta) = d\sigma/d\Omega(\theta, \hat{n}_1 \cdot \hat{n}_2 = 1),$$

and

$$I_R(\theta) = d\sigma/d\Omega(\theta, \hat{n}_1 \cdot \hat{n}_2 = -1).$$

[12] H. R. Rugge, Ph.D. thesis, Lawrence Radiation Laboratory Report UCRL-10252, 1960 (unpublished).
[13] V. Zinov, A. Konin, S. Korenchenko, and B. Pontecorvo, Soviet Phys.—JETP 11, 1233 (1960).
[14] H. A. Bethe and P. Morrison, Elementary Nuclear Theory (John Wiley & Sons, Inc., New York, 1956), 2nd ed., pp. 133–142.

If we use Eq. (6), Eq. (7) reduces to

$$e(\theta) = P_1 P_2(\theta). \quad (8)$$

Equation (8) represents the asymmetry observable after two consecutive scatterings in the same plane, as shown in Fig. 6. Although the recoil-proton scattering angle θ_1 is to the right, the pion scatters to the left, and hence unit vector $\hat{n}_1$ is directed out of the paper, as is unit vector $\hat{n}_2$ for θ_2 left. It should also be noted that although the proton appears to scatter right in Fig. 6, the center-of-mass picture shown in Fig. 7 indicates that both pion and proton undergo a left scattering. The quantity P_2 for carbon is known, so one could in principle calculate P_2 for the system; however, since our counters have finite size, and the analyzing target consists partly of carbon and partly of scintillator (see counter B, Fig. 8), we chose to determine P_2 experimentally. This is discussed in Sec. IVB.

The angular region measurable with a carbon analyzing target is severely limited by the sharp drop in polarization of protons on carbon below proton energies of about 120 MeV. For the largest of our proton angles (about 32 deg lab), the energy of the recoil proton as it leaves the hydrogen target is only 130 MeV; we are therefore forced to use a thinner carbon target to minimize additional energy loss. This reduces the counting rate and makes measurement of polarization at larger angles impractical. Also, measuring polarization at angles less than 17 deg is hindered by the main pion beam hitting the one analyzing telescope.

Referring to Fig. 8, the recoil protons were defined by a coincidence of the form ABR_1R_2. Counters A and B counted the proton, and R_1 and R_2 the scattered pion. The requirement of R_1R_2 coincidence with AB sharply reduced the possibility of counting inelastic protons, because these would not usually obey the required kinematics. The protons were then scattered by the carbon target (and also, to some extent, by counter B), and the relative intensities into counters D_1E_1 and D_2E_2 were measured. In the orientation of Fig. 3, the quantity I_L of Eq. (7) is given by $(ABR_1R_2D_1E_1)/(ABR_1R_2)$, and I_R is given by $(ABR_1R_2D_2E_2)/(ABR_1R_2)$.

In the interest of reducing the accidental rate, counter F was placed in anticoincidence so that the number of triggers for counters D and E would be reduced to that number of recoil protons actually scattered out by counter B and the carbon target. The rate of $ABR_1R_2\bar{F}$
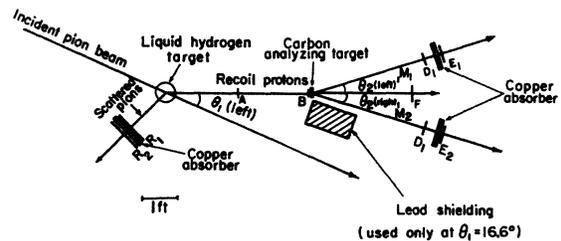

FIG. 8. Scale drawing (plan view) of counter arrangement.

TABLE V. Dimensions of counters used in polarization measurement.

Counter	Dimensions (in.)
A	1/4×2×6
B	1/4×2×8
R_1 and R_2	3/8×12×12
D_1 and D_2	3/4×4×20
E_1 and E_2	3/4×6×22
F	3/4×6×12
M_1 and M_2	1/4×1×6

compared to ABR_1R_2 was about 12%, i.e., $\approx 12\%$ of the protons scattered from the carbon target and counter B.

Counters M_1 and M_2 were used to monitor the center line of the recoil-proton beam, by moving them laterally until the rates $ABR_1R_2M_1$ and $ABR_1R_2M_2$ were approximately equal. Any deviations from equality during the course of a run then indicated a shift in center line.

2. Apparatus

The liquid-hydrogen target used was the same as described in Sec. IIIA.

The scintillation counters were mounted as shown in Fig. 9. Only the scintillator parts of each counter are shown. A transit was mounted directly above the pivot as shown; the angle θ_2 was then set by sighting on the centers of counters D_1 and D_2. Counters M_1 and M_2 had movement perpendicular to the beam line on a screw-driven table, which allowed setting to approximately 0.05 cm. Scintillator dimensions are given in Table V.

3. Counters and Electronics

All the counters were rectangular polystyrene scintillators connected through Lucite light pipes to RCA 6810-A photomultiplier tubes.

The negative output pulse from the phototube was then amplified and fed into Wenzel coincidence circuits.[10] Attempts to form a fourfold (ABR_1R_2) coincidence proved unsuccessful, owing to the significant time spread in R_1 and R_2 pulses with respect to A and B
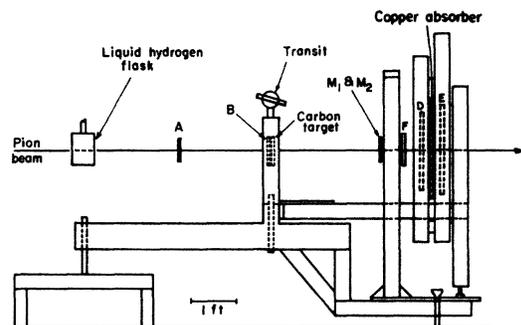

FIG. 9. Scale drawing (elevation view) of counters, including important supports. Counters R_1 and R_2 and supports are not shown.

pulses. Wherever counters of rather large dimensions were used (counters R, D, and E), it was necessary to form double coincidences of the form R_1R_2, D_1E_1, etc., and to mix the output of these doubles with the other pulses. The basic ABR_1R_2 coincidence was produced by two identical circuits; both these outputs were scaled, and one was used as a trigger for the remaining four types of coincidences $ABR_1R_2D_1E_1\bar{F}$, $ABR_1R_2D_2E_2\bar{F}$, $ABR_1R_2M_1$, and $ABR_1R_2M_2$.

B. Experimental Procedures

1. General

All the counters were first placed in the pion beam and the signals properly delayed. Voltage plateaus were also determined while the counters were still in the pion beam; then the delays were adjusted to compensate for the velocity difference between pions and recoil protons.

The apparatus was then moved to an angle θ_2 of about 20 deg, and the voltage plateaus were determined for protons. Copper absorber 1/2 in. thick was placed between counters R_1 and R_2 to reduce the number of low-energy particles giving an R_1R_2 coincidence. Copper absorber was also placed between counters D and E; the amount was determined by the procedure described in Sec. IVB-2.

When the voltage levels had been determined for all counters, all voltages were changed by ±50 V, which produced no change in counting rates. This check was repeated periodically throughout the experiment.

Accidental rates were determined by delaying counters D and E with respect to the $ABR_1R_2\bar{F}$ trigger by 54 nsec. This is the time difference between two radio-frequency fine-structure pulses of the cyclotron. The accidental counting rate was observed to be strongly dependent on the duty cycle of the cyclotron. In order to monitor the cyclotron duty cycle, the output of a scintillation counter placed in the main pion beam was displayed on an oscilloscope, and a continuous effort was made to keep the beam spread out over as long a time interval as possible.

TABLE VI. Asymmetry summary.

θ_1 (lab) (deg)	Telescope D_1E_1	Telescope D_2E_2	Average asymmetry[a]
16.6 L⎫	−0.092±0.047[b]	−0.183±0.050	−0.135±0.034
16.6 R⎭	0.235±0.067	0.143±0.050	0.177±0.040
22.1 L⎫	−0.192±0.049	−0.270±0.044	−0.236±0.033
22.1 R⎭	0.288±0.050	0.304±0.050	0.296±0.035
26.6 R[c]	0.366±0.046	0.377±0.041	0.371±0.031
31.6 L⎫	−0.295±0.060	−0.193±0.064	−0.248±0.044
31.6 R⎭	0.298±0.088	0.330±0.079	0.316±0.059

[a] The average asymmetry was obtained by combining the measurements of the two telescopes weighted by the inverse of the square of their errors. The error quoted is equal to $[(\Delta\epsilon_1)^{-2}+(\Delta\epsilon_2)^{-2}]^{-1/2}$, where $\Delta\epsilon_1$ and $\Delta\epsilon_2$ are the errors on the asymmetry measured by telescopes 1 and 2.
[b] All errors quoted on this page are based on counting statistics.
[c] Time limitations made it impractical to measure the asymmetry for $\theta_1 = 26.6$ deg L. In view of the good agreement between left and right at the other three angles, it was deemed unnecessary to make the measurement at $\theta_1 = 26.6$ deg L.

TABLE VII. Summary of pertinent quantities.

Quantity	Mean recoil-proton lab angle (deg)			
	16.6	22.1	26.6	31.6
c.m. scattering angle (deg)	145.2	133.8	124.5	114.2
Analyzing-telescope angle Q_2 (deg)	15.5	15.5	17.0	17.0
Thickness of carbon-analyzing target (in.)	2.0	1.0	0.5	0.5
Copper absorber thickness between counters D and E (g/cm²)	5.03	7.90	6.42	4.29
Approx. scattered-proton rate (ABC_1C_2) per minute	1250	900	680	650
Approx. average-analyzed proton rate ($ABC_1C_2DE\bar{F}$) per minute	3	1.3	0.7	0.9
Total number of full-normal counts recorded	2400	2200	1350	1250

At the smallest proton lab angle (16.9 deg) the accidental rate in the DE telescope nearest the main pion beam became prohibitive; this was improved by stacking lead between counter B and the main pion beam, which shielded the telescope from the hydrogen target.

Possible differences in efficiency between counter telescopes D_1E_1 and D_2E_2 were minimized by reversing the positions of the two telescopes regularly; the asymmetries measured by each telescope were then compared. The asymmetry measured by each telescope at each angle is recorded in Table VI, and the final asymmetry quoted at each angle is the average of the two telescopes.

Asymmetry was measured at equal angles to the left and right of the main pion beam. Since the unit vector $\hat{n}$, defined in Sec. IVA, is opposite in direction for these two scatterings, the preferred spin direction for a given value of polarization (P_1) also changes sign. The quantity P_2 remains the same, so the asymmetry as defined by Eq. (7) should also change sign. This was observed to be so, and is shown in Table VI.

2. Asymmetry Measurement

Counter telescope AB was positioned at each recoil angle by means of a transit on the pion beam center line, downstream from the hydrogen target. Counter B was beam defining, and the angle was set to about 0.05 deg. Counter telescope R_1R_2 was then set at the corresponding recoil-proton angle by means of an angle scale inscribed on the supporting table. This setting was accurate to about 0.2 deg.

The first measurement made at each recoil angle was a range determination using both counter telescopes D_1E_1 and D_2E_2. With the telescopes set at $\theta_2 = 0$ deg, the ratio $(ABR_1R_2DE)/(ABR_1R_2D)$ was measured and plotted against thickness of copper absorber between D and E. The range determined from these curves agreed well with kinematics, and agreement between the two DE telescopes was also good.

Examination of the tail of the range curves indicated that of the real ABR_1R_2D counts, only about 2% were particles of range greater than that of protons for this recoil angle. The "set point" indicates the amount of copper absorber placed between counters D and E during asymmetry measurements. This absorber was used in part to discriminate against protons that scatter inelastically from carbon and in part to reduce the number of DE coincidences from stray low-energy particles. The "set point" for each recoil angle is given in Table VII.

The center line of the recoil-proton beam was then determined for the two telescopes, by sweeping each telescope across the proton beam in 1-deg steps, and plotting $(ABR_1R_2DE)/(ABR_1R_2)$ against θ_2. The center line was determined to 0.05 deg. Checks were made frequently during the early stages of the experiment to ascertain the constancy of the center line. Later it was concluded that keeping the ratio $(ABR_1R_2M_1)/(ABR_1R_2M_2)$ between 0.90 and 1.10 guaranteed a shift in proton center line of less than 0.05 deg.

Telescopes D_1E_1 and D_2E_2 were then set at equal angles θ_2 measured from the center line as determined by the respective telescope, and the following four counting rates were measured:

(a) target full, delays normal;
(b) target full, DE delayed 54 nsec with respect to $ABR_1R_2\bar{F}$;
(c) target empty, delays normal; and
(d) target empty, DE delayed 54 nsec with respect to $ABR_1R_2\bar{F}$.

Rates (a) and (b) were monitored against the ABR_1R_2 rate, as well as against readings of an argon-filled ionization chamber placed in the main pion beam before the hydrogen target; rates (c) and (d) were monitored against the ionization chamber only.

At all angles, rate (c) was less than 4% of rate (a). At $\theta = 31.6$ deg, rate (b) was about 7% of rate (a), and at all other angles it was less than 5%. As a check on the validity of measuring accidentals in this manner, the beam was turned down to about 1.5×10^6 π/sec, and asymmetry was measured for $\theta = 31.6$ deg. Rate (b) dropped to less than 5%, but the net counting rates were unchanged. Rate (d) was in all cases less than 1%.

Table VII summarizes pertinent quantities for each of the angles measured.

3. Calibration

As mentioned in Sec. IVA, the quantity P_2 was determined experimentally for this counter arrangement. This calibration was carried out by Foote,[2] and is discussed very briefly here. The reader is referred to the above publication for a detailed account of the calibration procedure.

A beam of protons was scattered from a 1/2-in. carbon target at an angle of 13.8 deg. These scattered protons were then analyzed by the counter system under condi-

TABLE VIII. Polarization summary.

Center-of-mass angle (deg)	114.2	124.5	133.8	145.2
Average asymmetry[a]	0.269±0.037[b]	0.371±0.032	0.264±0.026	0.152±0.027
Analyzing ability[c]	0.344±0.034	0.573±0.046	0.449±0.032	0.500±0.020
Recoil-proton polarization	0.784±0.132	0.648±0.076	0.589±0.072	0.304±0.055

[a] This is the average of the two asymmetries measured by telescopes 1 and 2 given in Table VI. The individual quantities have been weighted by the inverse of the square of their errors.
[b] This quoted error in asymmetry includes the uncertainty of 0.09 due to center-line uncertainty (see Sec. IVC-2).
[c] This analyzing ability was measured by Foote (reference 2) and is the average of the values given in Table VI.

tions identical with that of the actual asymmetry measurements, as discussed in Sec. IVB2. This measured quantity e_2 is then equal to P_1P_2, where P_1 is the polarization of the once-scattered proton beam. P_1 was calculated from data of Dickson and Salter,[15] Tyrén et al.,[16] and Hafner.[17] The values of $P_2 = e_2/P_1$ quoted in Table VIII are the averaged values given in Foote.[2]

C. Polarization Results and Experimental Uncertainties

1. Results

Table VI presents the measured asymmetries as determined by the two telescopes for θ_1 to the left and right. The results from the two telescopes are averaged, and the values for θ_1 left and right are in turn averaged and listed in Table VIII.

2. Uncertainties

The principal sources of error in the asymmetry measurements are from counting statistics and uncertainty in recoil-proton beam center line. Counting statistical errors in asymmetry are related to errors in I_L and I_R [see Eq. (7)] by[18]

$$\Delta e \approx \frac{1-e^2}{2}\left[\left(\frac{\Delta I_L}{I_L}\right)^2 + \left(\frac{\Delta I_R}{I_R}\right)^2\right]^{1/2}.$$

These errors are quoted in Table VII.

Uncertainty in asymmetry due to uncertainty in center line is related to angular uncertainty by[18]

$$de/d\theta_2 \approx d(\ln I_0)/d\theta_2,$$

[15] J. M. Dickson and D. C. Salter, Nuovo Cimento 6, 235 (1957).
[16] H. Tyrén and Th. A. J. Maris, Nucl. Phys. 4, 637 (1957); P. Hillman, A. Johansson, and H. Tyrén, ibid. 4, 648 (1957); Th. A. J. Maris and H. Tyrén, ibid. 4, 662 (1957); R. Alphonce, A. Johansson, and G. Tibell, ibid. 4, 672 (1957).
[17] E. M. Hafner, Phys. Rev. 111, 297 (1958).
[18] T. J. Ypsilantis, Ph.D. thesis, University of California Radiation Laboratory Report UCRL-3047, 1955 (unpublished).

where I_0 is the average differential cross section for scattering at a lab angle θ_2 (see Fig. 8). For the geometries used in the aforementioned experimental arrangements, $de/d\theta_2 \approx 0.2/\text{deg}$.

As stated in Sec. IVB-2, the recoil-proton beam center line was determined to about 0.05 deg from the umbra curves. The monitor counters M_1 and M_2 guaranteed the constancy of the beam center line during the course of any run. The transit made angle settings possible to about 0.02 deg, a negligible contribution to the uncertainty. From these considerations, the rms error due to center-line uncertainty was $\Delta e \approx 0.010$. This error was added in rms fashion to the counting statistical uncertainties, and quoted in Table VIII.

The mean recoil-proton lab angle is assumed known to 0.40 deg. This uncertainty arises partly from uncertainty in the pion-beam center line, and partly from the calculation needed to determine the mean lab angle from the actual center line of counters A and B (necessitated by the variation of the differential cross section across the finite size of counters A and B). The incident-pion-beam center line was determined to 0.3 deg, and the setting of the A-B center line by transit was dependable to about 0.1 deg. The pion beam was centered on the liquid-hydrogen target at the beginning of each day by methods outlined in Sec. IIB so that daily variations of beam center line were minimized.

FIG. 1. Beam layout.